Eur. J. Mech. B - Fluids 20 (2001) 415–425
© 2001 Éditions scientifiques et médicales Elsevier SAS. All rights reserved
S0997-7546(01)01132-3/FLA

Model analysis of aspects of the flow field ahead of a density current

Carlos Härtel

Institute of Fluid Dynamics, ETH-Zentrum, CH-8092 Zürich, Switzerland

(Received 3 March 2000; revised 10 October 2000; accepted 5 January 2001)

Abstract – A potential-flow configuration consisting of an arrangement of point sources is employed to model the flow ahead of a density current in a plane channel. The model is used to examine two aspects of the flow, namely the magnitude of the velocities induced by the propagating front, and the deceleration that the front experiences when it approaches a vertical barrier from a distance. Concerning the induced velocities, simple relations are derived which show that the magnitude of these velocities is not only a function of the distance from the nose, as assumed in the past. Rather, it also depends on the fractional depth of the front, i.e. the ratio of front height to channel height. Concerning the deceleration of a front approaching an end wall, we show that for distances large compared to the channel height, the front slows down at an exponential rate. On the other hand, an algebraic relation is found in the region close to the end wall. It is demonstrated that the change in front speed due to the presence of an end wall remains negligibly small for distances between front and end wall larger than about two front heights. A comparison of the present analytical results with experiments and direct numerical simulations shows close agreement. © 2001 Éditions scientifiques et médicales Elsevier SAS

density currents / potential flow

1. Introduction

Density currents or gravity currents are common flow phenomena in many natural and man-made situations [1]. Such flows are driven by differences in hydrostatic pressure which are caused by density differences between the current and the ambient fluid. For example, in atmospheric gravity currents like sea-breeze fronts, density differences are typically caused by the difference in temperature between the spreading cold front and the relatively warmer ambient air. Gravity currents are most often encountered in geophysical applications, but their study is of relevance also in the engineering sciences because of the important role they play in many problems related to industrial safety and environmental protection [1,2].

In the present paper we will investigate aspects of the flow ahead of density currents, considering the generic case of a front traveling in a plane channel sketched in *figure 1*. The first issue we will address is the magnitude of the 'disturbance velocity' that a density current propagating into a large body of quiescent fluid induces in the region ahead of its nose. This problem has been studied previously by Middleton [3] who found that – for the cases considered in his experiments – the maximum of the induced velocity decays away exponentially with increasing distance from the nose. However, the range of validity of the exponential law or details of the functional dependence of this law on the governing flow parameters could not be disclosed. In the present analysis we will reconsider this problem with the aim to develop a more complete picture. In particular, we attempt to elucidate the role that the fractional depth of the front plays, which is the ratio of front height to channel height. The analysis we perform will include the relevant case of a front propagating in an environment which is unbounded in the vertical direction, i.e. where the fractional depth approaches zero. This situation applies, for example, to dense-gas fronts spreading in the open atmosphere.

E-mail address: Carlos.Haertel@ifd.mavt.ethz.ch (C. Härtel).

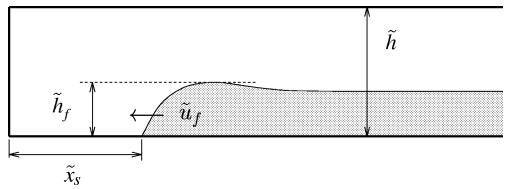

Figure 1. Principle sketch of a gravity current of height $\tilde{h}_f$ propagating in a channel of height $\tilde{h}$. The speed of the front is denoted as $\tilde{u}_f$, while $\tilde{x}_s$ is the distance between the foremost point of the front and an end wall.

The second aspect we wish to study is the problem of how a propagating front slows down when it approaches an end wall from a distance. We emphasize, however, that we are not interested in the immediate collision process between the front and the barrier. Rather, we are concerned with the nature of the interaction before collision, i.e. we seek to clarify how the front is gradually retarded with decreasing distance from the wall. Among other things, our motivation for studying this problem relates to the fact that in practice gravity currents often spread in environments that are virtually unbounded in the flow direction, as is the case, e.g., for smoke spreading in long rail-road tunnels [4]. On the other hand, in laboratory studies or in numerical simulations, the flow domain inevitably has to be bounded in the direction of propagation. This raises the question of how long the flow domain needs to be, to make sure that end-wall effects can safely be neglected. In the present analysis, the influence of the end boundary will be discussed in terms of the changes in front speed $\tilde{u}_f$ (a tilde indicates a dimensional quantity here). We will quantify this influence by an 'error' $\varepsilon_f = |\tilde{u}_{f,\infty} - \tilde{u}_f|/|\tilde{u}_{f,\infty}|$, where $\tilde{u}_{f,\infty}$ denotes the speed at which the front would propagate if the channel was infinitely long. What we aim at is to determine how ε_f depends on the distance between front and end boundary, and, again, on the fractional depth of the front.

To approach the above issues theoretically, we construct a flow model which is sufficiently simple to allow for solutions in closed form while retaining the essence of the problem under consideration. The fundamental assumption made is that for both issues studied here, the details of the flow in the source region are much less relevant to the problem than the flow state at the foremost part of the front. For example, concerning the end-wall effects this corresponds to the assumption that the front is not equally retarded over its full length, but that the decay in front speed is primarily caused by a local deformation of the flow pattern at the leading edge which is first exposed to the pressure rise. In the following section we will present a potential-flow configuration which generates a flow that bears strong resemblance to the flow at the foremost part of a gravity current (and ahead of it) and is able to effectively mimic the flow in this region. We stress, however, that this potential flow is in fact a *model* and, hence, needs to be validated carefully. To this end, we will undertake comparisons of the model predictions with available experimental results and accurate reference data obtained from direct numerical simulations.

2. Potential flow model

The two-dimensional potential-flow model that we employ for our analysis is sketched in *figure 2*. As basic elements we have a parallel flow $\tilde{u}^p$ in the longitudinal direction $\tilde{x}$ and an array of an infinite number of sources of strength $\tilde{Q}$ which are placed at $\tilde{x} = 0$ with a distance of $2\tilde{h}$. The flow field $\tilde{u}^q, \tilde{v}^q$ induced by the sources has symmetry planes aligned with $\tilde{x}$ which will subsequently play the role of the top and bottom walls of the channel. The complex potential Φ^q of the array of sources in *figure 2* can be obtained by a conformal mapping [5] and reads

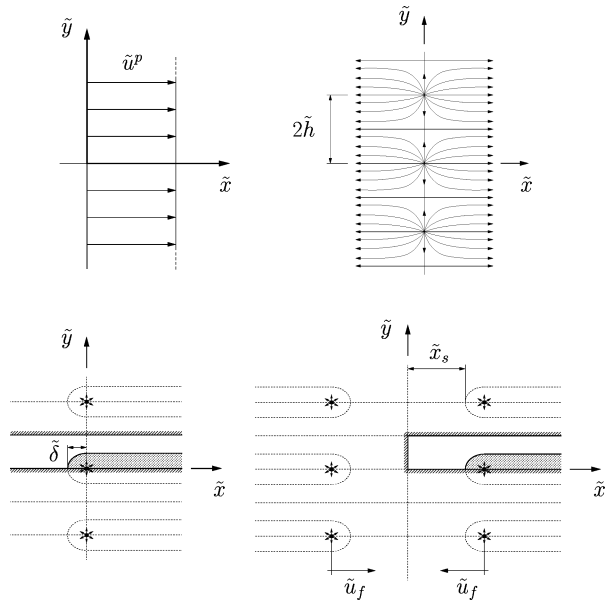

Figure 2. The basic elements of the potential-flow model are a parallel flow $\tilde{u}^p$ (top left) and an array of sources of strength $\tilde{Q}$ (top right). The superposition results in a flow that resembles the foremost part of a propagating front in a plane channel (bottom left; source positions are indicated by dots with arrows). The influence of an end wall on the front can be studied, if a vertical symmetry plane is introduced as shown in the bottom right graph. To this end two arrays of sources are moved in from $\tilde{x} = \pm\infty$ at speed $\tilde{u}_f$. In the figure shaded and hatched areas indicate the front and the walls of the channel, respectively.

$$\Phi^q = \frac{\tilde{Q}}{4\pi} \ln\left[4\left(\sin^2\left(\frac{\pi}{2}\frac{\tilde{y}}{\tilde{h}}\right) + \sinh^2\left(\frac{\pi}{2}\frac{\tilde{x}}{\tilde{h}}\right)\right)\right] + i \cdot \frac{\tilde{Q}}{2\pi} \arctan\left[\frac{\tan\left(\frac{\pi}{2}\frac{\tilde{y}}{\tilde{h}}\right)}{\tanh\left(\frac{\pi}{2}\frac{\tilde{x}}{\tilde{h}}\right)}\right], \tag{1}$$

where $i = \sqrt{-1}$. In the present analysis, we will only consider the flow state along the stagnation streamline where the velocities induced by the front are largest. Also, to determine the front speed, only the position of the foremost point of the front must be followed, which is precisely the stagnation point located in the symmetry plane. Therefore, we will concentrate on the flow at $\tilde{y} = 0$ in the remainder. In this plane $\tilde{v}^q = 0$, while $\tilde{u}^q$ is given by

$$\tilde{u}^q(\tilde{x}, \tilde{y} = 0) = \frac{\tilde{Q}}{4\tilde{h}} \coth\left(\frac{\pi}{2}\frac{\tilde{x}}{\tilde{h}}\right), \tag{2}$$

which has the limit

$$\tilde{u}^q_\infty = \lim_{\tilde{x}\to\infty} \tilde{u}^q(\tilde{x}, \tilde{y} = 0) = \frac{\tilde{Q}}{4\tilde{h}}. \tag{3}$$

Note that $\tilde{u}^p$ must be larger than $\tilde{u}^q_\infty$, if the superposition of the parallel flow and the sources is to provide a flow field similar to the one sketched in the lower-left graph of *figure 2*. In the vicinity of the source and to the right, the model flow is different from a gravity current, but near the leading edge and ahead of it, a stagnation-point flow is encountered which resembles the flow at the foremost part of an intrusion front [1,6]. This similarity of the flow topology at the leading edge is what is most relevant for the present study. Note, however, that the outline of the leading edge in the present model somehow differs from the more wedge-like shape of a gravity-current head. Although this difference may bear relevance for some aspects of the flow in the neighborhood of

the leading edge, it does not have a noticeable effect on the flow features we wish to study, as will become clear from the comparison with simulation results in section 5.

For large distances from the source, the velocity $\tilde{u} = \tilde{u}^p + \tilde{u}^q$ has the limits $\tilde{u}^p \pm \tilde{u}^q_\infty$ for $\tilde{x} \to \pm\infty$. The limit to the left is the actual speed of the front, i.e. $\tilde{u}_{f,\infty} = \tilde{u}^p - \tilde{u}^q_\infty$, where the subscript ∞ in $\tilde{u}_{f,\infty}$ indicates that this is the front speed in an infinitely long channel. The limit to the right, on the other hand, can be employed to derive a relation for the height of the front $\tilde{h}_f$. If we take the front height to be the distance in normal direction between the symmetry plane at $\tilde{y} = 0$ and the streamline that separates the oncoming fluid from the fluid issuing from the source, we find

$$\tilde{h}_f = \frac{\tilde{Q}}{2(\tilde{u}^p + \tilde{u}^q_\infty)}. \tag{4}$$

Similarly, the front position is defined by the foremost point that the fluid originating from the source may reach. This foremost point is the stagnation point located some distance $\tilde{\delta}$ ($\tilde{\delta} > 0$) to the left of the source. Note that in the present potential-flow model the position of the front or its height cannot be derived from a density field, since density differences are not taken into account.

For non-dimensionalization we employ $\tilde{u}_{f,\infty}$ as the reference velocity together with the front height $\tilde{h}_f$ as the reference length. The dimensionless velocity $u(x)$ at $y = 0$ then reads

$$u(x) = \frac{2-\kappa}{2-2\kappa} + \frac{\kappa}{2-2\kappa}\coth\left(\frac{\pi}{2}\kappa x\right), \tag{5}$$

where $\kappa = \tilde{h}_f/\tilde{h}$ is the fractional depth of the front. The non-dimensional distance δ between source and foremost point of the front is implicitly given by the condition $u(x = -\delta) = 0$. By virtue of (5) one finds

$$\delta = -\frac{1}{\pi\kappa}\ln(1-\kappa). \tag{6}$$

3. The flow field ahead of the current

From equation (5) we can compute the magnitude of the velocity that a gravity current propagating into quiescent fluid will induce in the region ahead of its nose. Measurements of these velocities were made by Middleton [3] who studied particle-driven gravity currents formed by releasing suspensions of plastic beads in a 5 meters long flume. The motion of the water ahead and around the developing front was then analyzed by tracing the movement of dye lines and dye spots from the individual frames of 16 mm movies of the experiments. Middleton gave his results in a laboratory frame of reference where the front moves while the fluid reservoir at large distances ahead of the front is at rest. To simplify the comparison with his data, (5) can be transformed into a frame of reference moving to the left at the non-dimensional front speed $u_f = 1$. The transformed velocity u^* in this translating system is given by $u^*(x) = u(x) - 1$. If we introduce $x_d = -x - \delta$ as a measure of the distance between the leading edge and some point x ahead of the front, we obtain from (5) for the magnitude $|u^*|$ of the induced velocity

$$|u^*(x_d)| = 1 - u(x_d) = \frac{\kappa}{2-2\kappa}\left[\coth\left(\frac{\pi}{2}\kappa(\delta + x_d)\right) - 1\right], \tag{7}$$

which, by virtue of (6), simplifies to

$$|u^*(x_d)| = \frac{\kappa}{\kappa - 1 + \exp[\pi\kappa x_d]}. \tag{8}$$

Middleton found that the maximum of the induced velocity (which, due to the no-slip condition, occurred a very short distance above the bottom wall in his experiments) decays exponentially with increasing distance from the leading edge. In our notation, his result reads

$$|u^*(x_d)| = C_1 \mathrm{e}^{-C_2 x_d} \tag{9}$$

with two non-negative constants C_1, C_2. Equation (9) agrees with (8) if in the denominator $(\kappa - 1)$ is neglected, which is justified for sufficiently large arguments $\pi\kappa x_d$. This yields

$$|u^*(x_d)| \approx \kappa \mathrm{e}^{-\pi\kappa x_d}, \tag{10}$$

showing that both $C_1 = \kappa$ and $C_2 = \pi\kappa$ depend on the fractional depth κ of the front. It is interesting to note that this dependence was left unnoticed in [3], although the slopes C_2 of the experimentally obtained curves feature systematic variations for varying fractional depths. Values of κ ranged between 0.3 and 0.4 in Middleton's experiments which, according to (10), corresponds to slopes C_2 roughly ranging between 0.8 and 1.2. This is remarkably close to the minimum and maximum slopes of the curves shown in [3] which are about 0.8 and 1.3, respectively.

Due to the pronounced lobe-and-cleft structure present at the leading edge, it is difficult in an experiment to measure accurately how u^* depends on x_d close to the front. In [3] it was assumed that (9) remains valid up to the leading edge, which implies $C_1 = 1$. However, the present results indicate that the exponential dependence does not hold for distances from the leading edge which are small compared to the channel height. For $\pi\kappa x_d \ll 1$, the leading-order approximation to equation (8) yields

$$|u^*(x_d)| \approx \frac{1}{1 + \pi x_d}, \tag{11}$$

which shows that in this case the decay of the disturbance with increasing distance from the leading edge is in fact not exponential, but rather algebraic. Note that in the limiting case of a front propagating in infinitely deep surroundings, where $\kappa = 0$, the relation (11) is valid for all x_d.

4. End-wall effects on the front speed

The potential-flow configuration is now employed to analyze the influence of an end wall ahead of the front on the front speed. To model the end wall, a vertical plane of symmetry must be introduced by using two arrays of sources, rather than one, which move towards each other at speed unity (see bottom right graph of *figure 2*). For deriving the resulting flow field, like in section 3 we first have to transform the velocity (5) into a translating system that moves to the right at speed unity. As the transformed coordinate x we will now use $x = x + x_q$, where $x_q(t)$ is the actual position of the source array that moves in from the right. The transformed velocity u^* in the translating system is given by $u^*(x) = u(x) - 1$, and its mirror image u^{**}, which needs to be added to obtain the plane of symmetry at $x = 0$, is given by $u^{**}(x) = 1 - u(-x)$. If we denote the sum of u^* and u^{**} by

u, we find

$$u(x, x_q) = \frac{\kappa}{2(1-\kappa)}\left[\coth\left(\frac{\pi}{2}\kappa(x - x_q)\right) + \coth\left(\frac{\pi}{2}\kappa(x + x_q)\right)\right]. \tag{12}$$

With the velocity field known, the propagation speed of the foremost point of the front, which is required to compute ε_f, can be evaluated in closed form. To this end, first the location x_s of the foremost point must be known, which is implicitly determined by the condition $u(x_s, x_q) = -1$. Applied to (12) this condition yields the following relation between x_q and x_s

$$\coth\left(\frac{\pi}{2}\kappa(x_s - x_q)\right) + \coth\left(\frac{\pi}{2}\kappa(x_s + x_q)\right) = -\frac{2(1-\kappa)}{\kappa}, \tag{13}$$

which may be rearranged to derive the explicit functional form of $x_s(x_q)$. The actual front speed $u_f = \mathrm{d}x_s/\mathrm{d}t$ can then finally be computed by the aid of the chain rule

$$u_f = \mathrm{d}x_s/\mathrm{d}t = \mathrm{d}x_s/\mathrm{d}x_q \cdot \mathrm{d}x_q/\mathrm{d}t = -\mathrm{d}x_s/\mathrm{d}x_q. \tag{14}$$

In terms of the non-dimensional quantities, the error is thus given by

$$\varepsilon_f = 1 - |u_f| = 1 + \mathrm{d}x_s/\mathrm{d}x_q. \tag{15}$$

If u_f is determined directly from equation (13), a very cumbersome formula is obtained which we will not present here. However, for illustration *figure 3* gives a result obtained from equation (13) for a fractional depth of 0.05, i.e. for a front traveling in a channel which is $20\tilde{h}_f$ deep. It is readily seen from the curve that ε_f, similar to the induced velocity discussed previously, falls off exponentially for large distances between front and end wall. In the next section we will separately consider the two limiting cases where x_s is either very small or very large compared to the channel height, i.e. where $\kappa x_s \ll 1$ and $\kappa x_s \gg 1$, respectively. For both cases approximations of the terms in (13) can be employed which allow the derivation of simple relations between ε_f and x_s.

With a relation for the front speed of the potential-flow configuration given, we can proceed to clarify the point made initially, namely how large the distance x_s in an experiment or simulation needs to be to ensure

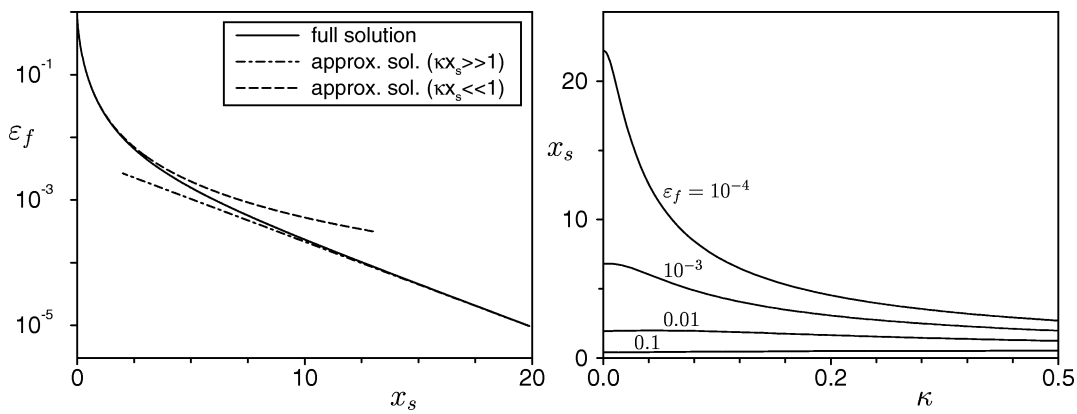

Figure 3. Left: Relative error ε_f in front speed $\tilde{u}_f$ as function of x_s. Results for a fractional depth of $\kappa = 0.05$. Given is the full solution based on equation (13) together with the near-field approximation (19) and the far-field approximation (30). Right: Minimum distance x_s required to ensure that ε_f remains below given thresholds of 0.01%, 0.1%, 1%, and 10%, respectively (results given in dependence on the fractional depth).

that undesired end-wall effects remain negligible. For fractional depths κ ranging between 0 and 0.5, we have evaluated from equation (13) the distance between front and end wall where ε_f reaches given threshold values between 0.01% and 10%, and the respective results are summarized in the right graph of *figure 3*. It is seen that the required minimum distance x_s strongly depends on κ if ε_f is to be extremely small. The smaller the fractional depth, the larger x_s has to be to guarantee that a maximum tolerable error is not exceeded. However, in most experimental studies or numerical simulations errors of the order of, say, 1% are certainly acceptable, and in this case a minimum distance of no more than about two front heights is required, almost independent of the fractional depth.

4.1. The near-field approximation ($\kappa x_s \ll 1$)

For distances between front and end wall which are small compared to the channel height $\tilde{h}$, an approximation of the relation $\varepsilon_f(x_s)$ is readily obtained if the terms on the left-hand side of equation (13) are simplified by means of a first-order Taylor series expansion for the hyperbolic cotangent. This gives

$$\frac{1}{x_s - x_q} + \frac{1}{x_s + x_q} = -\pi(1-\kappa). \tag{16}$$

The above quadratic equation has two solutions $x_s(x_q)$. The relevant one of these is found from the constraint $x_s \geqslant 0$ and reads

$$x_s = \frac{1}{\pi(1-\kappa)}\Big(\sqrt{1+(1-\kappa)^2\pi^2 x_q^2} - 1\Big). \tag{17}$$

The error in front speed is now obtained from (17) by virtue of equation (14) which yields

$$\varepsilon_f = 1 - \frac{\pi(1-\kappa x_q)}{\sqrt{1+(1-\kappa)^2\pi^2 x_q^2}}. \tag{18}$$

As a final step one has to employ equation (17) to express x_q as a function of x_s, which results in an algebraic relation for the error ε_f as a function of the distance x_s between front and end wall

$$\varepsilon_f = 1 - \sqrt{1 - \frac{1}{(1+(1-\kappa)\pi x_s)^2}}. \tag{19}$$

Clearly, the extent of the neighborhood of the wall where equation (19) is a valid approximation must depend on the actual value of κ. Since it was derived under the assumption $\kappa x_s \ll 1$, equation (19) can be applied to an ever larger flow region adjacent to the end boundary if the fractional depth decreases. For illustration, we have included the approximate solution for $\kappa = 0.05$ in *figure 3*, and a close agreement with the full solution is seen for distances up to at least $x_s \approx 4$. Note that, like in section 3, the near-field approximation becomes in fact the exact solution in the limiting case of a front propagating in infinitely deep surroundings where $\kappa = 0$.

4.2. The far-field approximation ($\kappa x_s \gg 1$)

The derivation of a simplified solution for large distances is slightly more involved, and as a first step we will introduce as a small quantity the difference Δx_s between the actual distance $(x_q - x_s)$ and the distance δ for a single source array given in (6), i.e. $\Delta x_s = \delta - (x_q - x_s) \ll 1$. Using Δx_s, and (6) along with a common relation for the hyperbolic cotangent of a sum, the first term on the left-hand side of (13) can be rewritten as

$$\coth\left(\frac{\pi}{2}\kappa(x_s - x_q)\right) = \frac{1 - \coth(\frac{\pi}{2}\kappa\Delta x_s)\coth(\frac{\pi}{2}\kappa\delta)}{\coth(\frac{\pi}{2}\kappa\Delta x_s) - \coth(\frac{\pi}{2}\kappa\delta)} \tag{20}$$

$$= \frac{1 - (2-\kappa)/\kappa \coth(\frac{\pi}{2}\kappa\Delta x_s)}{\coth(\frac{\pi}{2}\kappa\Delta x_s) - (2-\kappa)/\kappa}. \tag{21}$$

Using first-order Taylor series expansions, (21) can be simplified to

$$\coth\left(\frac{\pi}{2}\kappa(x_s - x_q)\right) \approx \frac{\pi\kappa\Delta x_s - 2(2-\kappa)/\kappa}{2 - (2-\kappa)\pi\Delta x_s}. \tag{22}$$

The second term on the left-hand side of (13) can be rewritten as

$$\coth\left(\frac{\pi}{2}\kappa(x_s + x_q)\right) = \coth\left(\frac{\pi}{2}\kappa(2x_q - \delta + \Delta x_s)\right) \tag{23}$$

$$\approx \coth\left(\frac{\pi}{2}\kappa(2x_q - \delta)\right). \tag{24}$$

Note that in (24) Δx_s has been neglected as a small quantity in the sum $2x_q - \delta + \Delta x_s$. By the aid of (6) the following relation can be derived from equation (24)

$$\coth\left(\frac{\pi}{2}\kappa(x_s + x_q)\right) = \frac{\kappa - (2-\kappa)/\kappa \coth(\pi\kappa x_q)}{\kappa\coth(\pi\kappa x_q) - (2-\kappa)}. \tag{25}$$

For $\kappa x_q \gg 1$ the hyperbolic cotangent in (25) is well approximated by

$$\coth(\pi\kappa x_q) \approx 1 - 2\exp[-2\pi\kappa x_q], \tag{26}$$

which yields

$$\coth\left(\frac{\pi}{2}\kappa(x_s + x_q)\right) \approx \frac{(\kappa-1) + (2-\kappa)\exp[-2\pi\kappa x_q]}{(\kappa-1) - (2-\kappa)\exp[-2\pi\kappa x_q]}. \tag{27}$$

Introducing (22) and (27) into (13) results in a relation that allows computing Δx_s as a function of the source position x_q and the fractional depth of the front κ

$$\Delta x_s = \frac{2\kappa}{\pi(\kappa^2 - (2\kappa^2 - 4\kappa + 2)\exp[2\pi\kappa x_q])}. \tag{28}$$

The time derivative of Δx_s, which is precisely the error ε_f, is then obtained by applying the chain rule similar to (14). This yields

$$\varepsilon_f = \frac{\mathrm{d}\Delta x_s}{\mathrm{d}t} = \frac{8\kappa^2(\kappa-1)^2\exp[-2\pi\kappa x_q]}{(2 - 4\kappa + 2\kappa^2 - \kappa^2\exp[-2\pi\kappa x_q])^2} \approx \frac{2\kappa^2}{(1-\kappa)^2}\mathrm{e}^{-2\pi\kappa x_q}, \tag{29}$$

which for $\Delta x_s \ll 1$ reduces to the following simple exponential dependence of ε_f on the distance x_s

$$\varepsilon_f(x_s) = 2\kappa^2\mathrm{e}^{-2\pi\kappa x_s}. \tag{30}$$

In *figure 3* we have included the respective result for the fractional depth of 0.05 and it is seen that the approximate solution (30) is indeed the proper approximation to the full solution for large x_s. Close agreement

between the two is observed from about $x_s = 10$ on. Clearly, like the approximate solution for $\kappa x_s \ll 1$, also equation (30) has a range of validity which depends on κ.

5. Simulation results

As pointed out before, the potential-flow configuration discussed in this paper is a 'model' rather than a rigorous 'theory' and therefore requires careful validation. In section 3 we have already discussed the good agreement between the model predictions and previous experiments on the flow field ahead of a gravity current. However, to our knowledge no measurements of end-wall effects are available that could be employed for comparison with our model analysis. Therefore, we have conducted direct numerical simulations (DNS) of viscous density currents in plane channels of finite length (see [7,8]). From the resulting DNS database, the front speed and the related end-wall effects can be determined with high accuracy. The basic set-up used in the simulations is depicted in *figure 4*. Initially the fluid in the rectangular flow domain is at rest, and in the right part of the channel a reservoir of height $\tilde{h}_r$ containing more dense fluid is provided. After the release a front forms which propagates to the left, as indicated by the dashed line in the figure. The Reynolds numbers of the flow, based on speed and height of the fronts, are about 1000. To study the influence of an end boundary numerically, simulations must be conducted in channels of widely differing length. Taking as the reference solution $\tilde{u}_{f,\infty}$

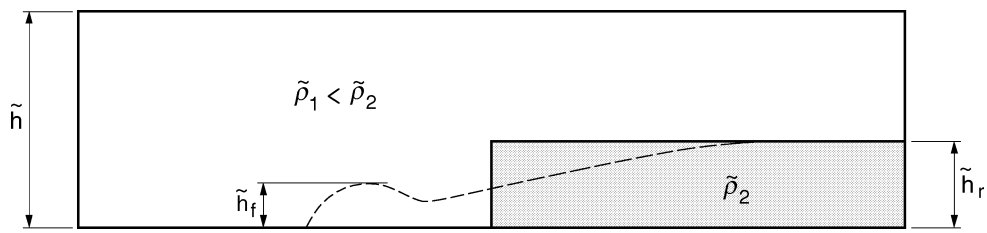

Figure 4. Set-up used in the DNS to generate an intrusion flow in a plane channel of height $\tilde{h}$. Initially the fluid is at rest and the more dense fluid is contained in a reservoir of height $\tilde{h}_r$. The dashed line shows the interface some time after the release when the front (height $\tilde{h}_f$) is already fully developed.

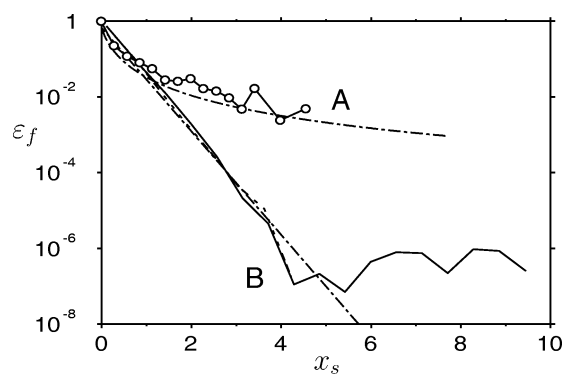

Figure 5. Relative error ε_f in front speed $\tilde{u}_f$ as obtained from direct numerical simulations of intrusion flows in a plane channel. (A) Shallow intrusion with $\kappa \approx 0.088$. The distance between the initial vertical interface and the end boundary was set to $\tilde{h}/2$ (reference solution obtained with a distance of $\tilde{h}$). The dot-dashed line gives the approximate solution (19) of the potential-flow model. (B) Lock-exchange flows with $\kappa \approx 0.55$ (see [8]). Results for different length $\tilde{L}$ of the computational domain: – – – $\tilde{L} = 5.25\,\tilde{h}$, —— $\tilde{L} = 10.45\,\tilde{h}$ (reference solution obtained in a channel of length $\tilde{L} = 15.7\,\tilde{h}$). For $x_s > 4$ the error falls below 10^{-6} which is approximately the noise level set by the numerical accuracy of the finite-difference scheme used to compute $\tilde{u}_f$. The approximate solution (30) is indicated by the dot-dashed line.

the front speed in the longest channel (which is least affected by the finite size of the computational domain), the error ε_f can then be evaluated from the relative difference in front speed between the reference solution and the solution obtained in the shorter channels.

The comparison of the DNS results with the potential-flow model is given in *figure 5* for two different cases. The first case is a lock-exchange flow where the fractional depth amounts to $\kappa \approx 0.55$. We remark that this is about the maximum fractional depth that can be realized in practice (see [9]). It is seen that the DNS data very closely follow the exponential curve given by equation (30) until the error becomes extremely small and falls below the numerical accuracy of the finite-difference scheme employed to compute $\tilde{u}_f$ from the simulation results. From the figure is it also recognized that for a lock-exchange flow the applicability of (30) is not constrained to large distances between front and end boundary, but the formula remains valid until the front has reached the immediate vicinity of the wall.

The second case shown in *figure 5* is a front that develops from a reservoir of height $0.1\tilde{h}$. In this case the associated front height varies with time more strongly than in the lock-exchange case, and we used the average of the instantaneous front height over the time interval of interest to determine κ. This lead to a fractional depth of 0.088. We remark that the computational costs for simulations of fronts originating from very shallow reservoirs are much higher than for lock-exchange simulations, due to the need to use a very extended computational domain. Therefore, we have restricted the validation in this case to a region between front and end wall which encompasses about 5–7 front heights, and where the near-wall approximation should hold. Like the lock-exchange flow, a good agreement between the model and the DNS data is also observed in this case, which impressively confirms the algebraic dependence (19) in the vicinity of the end wall.

6. Summary

We have presented a comparatively simple potential-flow configuration that can be used to examine aspects of the flow ahead of a density current propagating in a plane channel. Two issues were addressed, namely the magnitude of the velocity induced by the front and the problem of how a front is being retarded when it approaches an end wall from a larger distance. The potential-flow model consists of arrays of sources, and can be solved in closed form. It has been designed specifically to mimic the flow at the foremost part of a gravity current (and ahead of it), and – by construction – can only account for certain features of gravity-current fronts. However, the model has an impressive predictive power, and the analytical results derived in the present work agree closely with existing experimental results and accurate reference data obtained from high-resolution simulations.

The functional form derived for the induced velocities ahead of the front reveals that the magnitude of these velocities not only depends on the distance from the leading edge, but also on the fractional depth of the front. It was shown that in a region ahead of the front which is small compared to the channel height, the induced velocities decay away in an algebraic fashion. On the other hand, the decay is exponential for larger distances. A very similar picture emerged in the analysis of the end-wall effects where again approximate solutions were presented for the limiting cases of very large and very small distances between front and end wall, respectively. With an eye on experiments or simulations which inevitably have to deal with flow domains of finite length, we have addressed the point of how close a front may approach an end wall, before the presence of the wall has a noticeable effect on the flow evolution. It was shown that the minimum distance required to ensure that end-wall effects remain negligible is about two front heights, almost independent of the fractional depth.

Acknowledgments

The author wishes to thank F. Necker and Professor E. Meiburg for helpful comments on a draft version of this paper. The DNS have been conducted at the Swiss Center for Scientific Computing (CSCS) in Manno, TI.

References

[1] Simpson J.E., Gravity Currents, 2nd ed., Cambridge University Press, Cambridge, 1997.
[2] Fanneløp T.K., Fluid Mechanics for Industrial Safety and Environmental Protection, Elsevier Science B.V., Amsterdam, 1994.
[3] Middleton G.V., Experiments on density and turbidity currents. I. Motion of the head, Can. J. Earth Sci. 3 (1966) 523–546.
[4] Kunsch J.-P., Critical velocity and range of fire-gas plume in a ventilated tunnel, J. Atm. Env. 33 (1999) 13–24.
[5] Betz A., Konforme Abbildungen, Springer-Verlag, Berlin, 1948, p. 166.
[6] Härtel C., Meiburg E., Gravity Currents and Their Analysis by Direct Numerical Simulation, Fortschritt-Bericht 7-366, VDI-Verlag, Düsseldorf, 1999.
[7] Härtel C., Kleiser L., Michaud M., Stein C.F., A direct numerical simulation approach to the study of intrusion fronts, J. Eng. Math. 32 (1997) 103–120.
[8] Härtel C., Meiburg E., Necker F., Analysis and direct numerical simulation of the flow at a gravity-current head. Part 1: Flow topology and front speed for slip and no-slip boundaries, J. Fluid Mech. 418 (2000) 189–212.
[9] Britter R., Simpson J.E., Experiments on the dynamics of a gravity current head, J. Fluid Mech. 88 (1978) 223–240.